2024 American Control Conference (ACC)
July 8-12, 2024. Toronto, Canada

Enhancing Protein Crystal Purity through Adaptive Kinetic Monte Carlo Modeling and Control of Surface Morphology

Satchit Nagpal[1], and Joseph Sang-II Kwon[1]

Abstract— **The escalating demand for producing highly purified proteins, free from contaminants, is paramount in preparative chromatography. To effectively mitigate crystal impurities and establish optimal operational strategies for crystallization processes, it becomes imperative to comprehensively understand the influence of surface morphology on protein crystals. In the present study, we introduce a novel microscopic kinetic Monte Carlo (kMC) model, specifically designed to account for various growth regimes by incorporating surface thermodynamic effects related to different growth mechanisms. This innovation centers on an adaptive adsorption rate that redefines the driving force behind crystallization. To ensure the model's precision and relevance, we validate it with experimental findings. Subsequently, the confirmed kMC model, which forecasts kink density changes, surface morphology, and crystal growth rates under disturbances, is incorporated into a model-based control strategy. This method calculates an optimal input trajectory that facilitates the achievement of the desired kink density, thereby significantly reducing impurities during the crystallization process. This research offers a novel approach for controlling the growth of protein crystals. Furthermore, the stochastic model presents a valuable framework for enhancing the purity of proteins through tunable kink density of crystals, critical for the biotechnology and pharmaceutical industries.**

I. Introduction

Crystal morphology critically affects the key product specifications and characteristics of various pharmaceutical, food products, and other chemical products. For example, crystal morphology can dictate the activity of certain active pharmaceutical ingredients (APIs) [1], selectivity to specific downstream reactions [2], pharmaceutical bioavailability [3]. Even optoelectronic properties in the case of quantum dot crystals (QD) [4], [5], [6]. Since accurate prediction of crystal surface morphology is essential for fine-tuning the product specifications, it is important to develop a mechanistic understanding of the different factors affecting crystal morphology, resulting in an accurate prediction. Also, analyzing the effect of different operating conditions (e.g., temperature cooling curves, supersaturation level, and others) on crystal morphology enables the engineering of high-quality crystals suitable for drug systems, optoelectronics, and food products [7]. Some recent machine learning based and hybrid modleing approaches can identify latent chemical mechanisms and it gurantees system-to-system transfer learning capability [8], [9], [10].

In solution-based crystallization, supersaturation levels determine growth mechanisms, resulting in three primary regimes: spiral, step, and rough. Spiral growth occurs at low supersaturation, driven by growth unit (GU) attachment sites like kinks. Kinks, which are often formed by defects in the crystal lattice, provide sites for impurities to attach [11]. When impurity molecules or foreign particles are present in the crystallization solution, they can preferentially attach to kinks on the crystal surface [12], [13]. This attachment is facilitated by the reduced energy barrier for adhesion at kinks, making kink-rich regions more prone to impurity adsorption [14]. Kinks can hinder the growth of pristine crystal layers [15], [16]. As the crystal lattice extends, kinks act as barriers that slow down the advancement of well-ordered crystal faces [17]. This slowdown in growth at kinks can create regions with imperfect crystal structures, which are more likely to incorporate impurities during the crystallization process.

Kinks can trap impurities within the crystal lattice. As the crystal continues to grow, impurities that have attached to kinks may become buried within the crystal structure [18]. This entrapment can lead to impurity incorporation into the crystal lattice, reducing its purity [19]. To enhance the purity of protein crystals, it is essential to control and minimize the kink density on the crystal surface. Adjusting parameters such as temperature, supersaturation level, and growth rate can influence the prevalence of kinks. Fine-tuning these conditions can promote the growth of smoother, less kink-prone crystal surfaces [20]. Regularly monitoring the purity of the growing crystals through techniques like X-ray crystallography or spectroscopy can help identify and address impurity issues early in the crystallization process [21]. Stochastic techniques like kinetic Monte Carlo (kMC) simulations are valuable for modeling these morphologies. Unlike molecular dynamics (MD), kMC offers insights over larger dimensions and extended timescales, approximating atomistic events into mesoscopic ones [22], [23], [24].

To enhance purity, our research introduces a novel microscopic kMC model capable of predicting crystal growth rate and morphology across a wide range of concentration gradients and temperatures. This model considers the detailed surface attributes of crystals, including terraces, kinks, edges, adatoms, and vacancies. Capturing the interactions and dynamics of these attributes offers insights into step advancement, spiral growth, and roughening mechanisms. Furthermore, our kMC model integrates thermodynamic considerations based on supersaturation and attachment energies, allowing us to control the kink density which is dependent upon the temperature during solution-grown crystallization.

[1]Satchit Nagpal and Joseph Sang-II Kwon are with the Artie McFerrin Department of Chemical Engineering, Texas A&M University, College Station, TX 77840, USA. Emails: kwonx75@tamu.edu Joseph Sang-Il Kwon is the corresponding author.

979-8-3503-8265-5/$31.00 ©2024 AACC

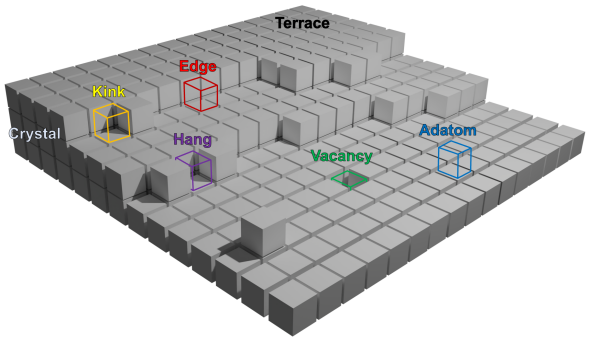

Fig. 1. Schematic illustration for a generalized faceted crystal with different adsorption sites.

II. Model Formulation

The kMC model simulates long-time dynamics using probabilistic rules and rate calculations from transition state theory (TST), facilitating the conceptualization of system transitions between discrete energy minimum states [25], [26]. Rate constants for transitions are determined by TST, which approximates the rate as equilibrium flux through a conceptual dividing surface, simplifying the complex dynamics of crystallization without needing explicit transition simulations.

We demonstrate the model's ability to connect different crystal growth regimes using the solid-on-solid (SOS) model, which represents the crystal surface as an array of columns with integer heights, excluding vacancy sites and considering factors like adatom clusters and step irregularities, as depicted in Fig. 1. Additionally, omitting variations in vibrational frequency and rotational free energy across different surface positions.

A. Microscopic model

In protein crystallization, particularly with larger molecules, such as proteins, the contribution of entropy due to solvent trapping or release plays a significant role [27]. The driving force for this process is primarily attributed to changes in surface free energy γ_{edge} during crystallization and the variation in chemical potential of the crystallizing solution, denoted as $\triangle\mu$. A higher magnitude of $\triangle\mu$ results in more pronounced crystal growth during the crystallization process [28], [29]. The $\triangle\mu$ for a supersaturated solution is defined as:

$$\triangle\mu = k_B T \ln \frac{C}{C_{eq}} \tag{1}$$

Here, k_B represents the Boltzmann constant, T denotes the temperature in Kelvin, C is the solute concentration, and C_{eq} represents the equilibrium solute concentration. For protein molecules, C_{eq} depends on the solution temperature [30].

The critical size l_c correlates surface morphology with supersaturation and predicts the different growth regimes observed. In the spiral growth regime, l_c becomes large, resulting in a smoother surface, unless a surface defect is present. In the step growth regime, clusters of islands are created, each being approximately the size of its critical size l_c. In the rough growth regime, the island size decreases until it is smaller than the unit GU size, leading to surface roughening. Clusters larger than this critical size have a higher probability of growing than decaying, while smaller clusters have a higher probability of decaying. To integrate this mechanism into the kMC model, we calculate the free energy change for each GU transfer during adsorption:

$$\triangle G_{GU} = -\triangle\mu + A_{GU}\gamma_{edge} \tag{2}$$

Here, A_{GU} represents the area gain due to GU attachment, and collectively, $A_{GU} \times \gamma_{edge}$ represents the bond energy for the GU. The attachment energy is dependent on the nearest neighbor count i for each adsorption site (adatom, step, kink, hang, vacancy):

$$A_{GU} = iA_f \tag{3}$$

where A_f is the area of each face for the GU. The time required for bond formation decreases with increasing bond energy. Thus, the adsorption rate of each GU depends on the free energy barrier:

$$r_a = K_a \exp\left(-\frac{\triangle G_{GU}}{k_B T}\right) \tag{4}$$

Desorption occurs when a GU breaks its interactions with the crystal surface and returns to the solvated state in solution. The desorption rate depends on the surface microconfiguration, and the total rate of desorption is:

$$r_{d_i} = K_0^+ \exp\left(\frac{\phi}{k_B T(t)} - i\frac{E_{pb}}{k_B T(t)}\right) \tag{5}$$

Migration, or surface diffusion, facilitates the movement of adsorbed GUs across the crystal surface without desorption. The migration rate is higher than the desorption rate and is defined as:

$$r_{m_i} = K_0^+ \exp\left(\frac{\phi}{k_B T(t)} - i\frac{E_{pb}}{k_B T(t)} + \frac{E_{pb}}{2k_B T(t)}\right) \tag{6}$$

This comprehensive model allows us to simulate the dynamic equilibrium between GUs and the crystal surface, incorporating adsorption, desorption, and migration processes. In case some therdodynamic parameters are not available from the literature, they can be obtained from DFT calculations and approaches described by Kwon and colleagues [31], [32].

B. Event execution

In the kMC simulation, we compute a time increment, $\triangle t_{kMC}$, after executing each event. This increment is determined based on the total rate of microscopic events, and it selects the time for the next event occurrence from a Poisson distribution:

$$\triangle t_{kMC} = -\frac{\ln(\zeta_t)}{W_{tot}} \tag{7}$$

Here, ζ_t is a uniform random number in the interval $\zeta_t \in (0, 1]$. The entire event execution cycle is depicted in Fig. 2,

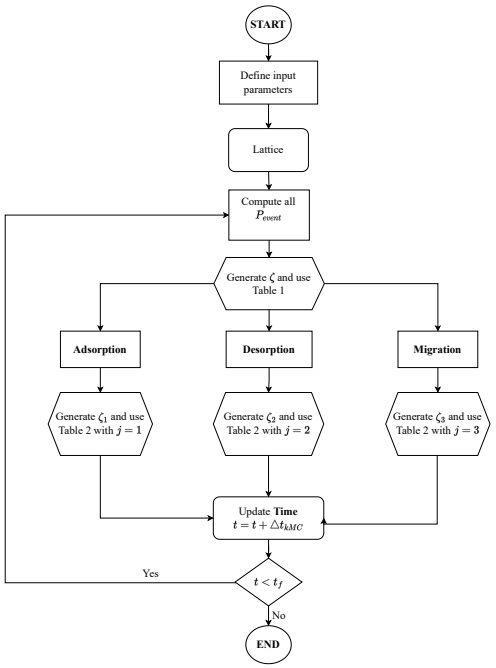

Fig. 2. Flow diagram of kMC algorithm adapted to simulate crystal growth

representing the kMC algorithm for each event and execution condition.

We utilize probabilities P_a, P_d, and P_m to determine which event to execute, as summarized in Table I. To select an event, we generate a uniform random number $\zeta_1 \in [0, 1)$. If $\zeta_1 \leq W_a/W_{tot}$, we execute an adsorption event. For $W_a/W_{tot} < \zeta_1 \leq (W_a+W_d)/W_{tot}$, we execute a desorption event. If $\zeta_1 > (W_a + W_d)/W_{tot}$, a migration event is executed. For adsorption, desorption, and migration, we also

TABLE I

PROBABILITY CONDITIONS FOR SELECTING A KMC EVENT.

Probability Conditions	Event Executed
$0 < \zeta \leq P_a$	Adsorption
$P_a < \zeta \leq P_a + P_d$	Desorption
$P_a + P_d < \zeta \leq P_a + P_d + P_m$	Migration

determine the specific class. In adsorption, we calculate the i^{th} class, an integer ranging from 0 to 4. Once the class is determined, a second random number is generated to select a random lattice site within class i for the desorption event. Desorption and migration events follow a similar process.

Table II illustrates the event selection conditions for all three events based on the number of nearest neighbors. For migration, lattice site classes are chosen based on direction, considering that a GU cannot migrate to a higher step. We first randomly select a direction and then check if migration is feasible. If not, no event occurs, but the time is still updated. An available migration site refers to the nearest neighboring site that is lower in height than the current lattice site, and each available migration site is equally likely to accept the displaced particle, following the approach by Bennema and colleagues [33].

TABLE II

PROBABILITY CONDITIONS FOR SELECTING A PROTEIN CASE i WITH AN EVENTS.

Probability Conditions	Number of Neighbors
$0 < \zeta_j \leq \frac{r_j(0)}{\sum_{i=0}^{4} r_j(i)}$	Zero
$\frac{r_j(0)}{\sum_{i=0}^{4} r_j(i)} < \zeta_j \leq \frac{\sum_{i=0}^{1} r_j(i)}{\sum_{i=0}^{4} r_j(i)}$	One
$\frac{\sum_{i=0}^{1} r_j(i)}{\sum_{i=0}^{4} r_j(i)} < \zeta_j \leq \frac{\sum_{i=0}^{2} r_j(i)}{\sum_{i=0}^{4} r_j(i)}$	Two
$\frac{\sum_{i=0}^{2} r_j(i)}{\sum_{i=0}^{4} r_j(i)} < \zeta_j \leq \frac{\sum_{i=0}^{3} r_j(i)}{\sum_{i=0}^{4} r_j(i)}$	Three
$\frac{\sum_{i=0}^{3} r_j(i)}{\sum_{i=0}^{4} r_j(i)} < \zeta_j \leq 1$	Four

III. DETERMINING OPTIMAL OPERATING STRATEGY FOR CRYSTALLIZER

The aim is to establish an optimal operational approach for the batch crystallizer, ensuring the achievement of the target kink density by the completion of the process. The subsequent section outlines the specific methodologies employed to derive this optimal strategy.

A. Stochasticity reduction

The inherent stochasticity of high-fidelity microscopic kMC simulations renders them impractical for solving optimization problems necessary to determine an optimal operational strategy. Consequently, we solved this challenge by running 10 independent simulations with the same operating conditions to reduce the stochastic fluctuations for kink density.

Our crystallization control strategy leverages the IPOPT solver for its adept handling of nonlinear optimization, ensuring effective solution finding within the complex crystallization process. Utilizing a branch and bound technique, we quantify the global optimality gap, affirming solution quality. The optimization targets completion within 1 hour, incorporating a 10-minute control horizon and a 1-minute time average for stochasticity reduction to stabilize kink density predictions. A key operational constraint includes maintaining the jacket control temperature adjustment rate at $2°C/min$, and optimizing crystal purity while avoiding thermal stress. This integrated approach combines computational efficiency with precise operational planning, aiming for high-purity protein crystals.

To run the optimization and control strategies, a sequence of inputs is gathered from the high-fidelity microscopic model, and the resulting outputs are utilized in conjunction and then averaged for the whole control horizon set to 10 minutes. This process leads to the development of a model predictive control (MPC) that can mitigate the inherent noise from the kMC simulations, represented as:

$$\begin{aligned} \kappa(t_k) &= \sum_{i=1}^{n} \kappa(t_{k_i}) \\ \kappa(t_k + \triangle t_c) &= \sum_{j=k}^{\triangle t_c} \kappa(t_{j_k}) \end{aligned} \tag{8}$$

Here, κ denotes the controlled variable of kink density, determined by counting the frequency of GUs with two neighbors. Meanwhile, $\triangle t_c$ signifies the control horizon, over which we compute a time average, yielding the model's kink density value. This is subsequently compared with the setpoint during each step of the optimization process.

B. Optimal operation of crystal growth

In this study, we tackle the challenge of achieving specific targets for the kink density of protein crystals by formulating an optimization problem, as shown in Eq. 9.

The optimization process involves determining the optimal input trajectory, which is then implemented in our high-fidelity kMC model, serving as a virtual experimental platform. Eq. 9 incorporates key parameters: T_i denotes the temperature at $t = t_i$, C represents the concentration of lysozyme in solution, and N signifies the length of the operation horizon.

The optimization problem addresses temperature as the manipulated input. Temperature is adjusted every minute, while the lysozyme concentration remains constant. This control optimization aims to achieve the following setpoint: $[\kappa_{sp} = 0.158]$.

$$\begin{aligned} \min_{T_1,\ldots,T_N} \quad & \sum_{i=1}^{N} F_\kappa \\ \text{s.t.} \quad & F_\kappa = (\kappa(t_N) - \kappa_{sp})^2 \\ & \kappa_i = f_r(T, C, t_i) \\ & 4^\circ C \leq T_i \leq 25^\circ C \\ & \left| \frac{T_{i+1} - T_i}{\triangle} \right| \leq 2^\circ C/min \end{aligned} \tag{9}$$

IV. Simulation Results

This section presents the validation of the developed kMC model for growth rates and a comparison with the existing kMC model. Further, the surface morphology for different growth regimes is visualized.

A. Validation of the layered-kMC simulations

Crystal growth rates were analyzed across protein solute concentrations from 30.0 to 135.0 mg/mL, with a solubility of 15 mg/mL. Parameters E_{pb}/k_BT and ϕ/k_BT were optimized using a grid search to align calculated and experimental growth rates, resulting in $E_{pb}/k_BT = 0.48$ and $\phi/k_BT = 3.76$ for face (110), and $E_{pb}/k_BT = 2.12$ and $\phi/k_BT = 4.27$ for face (101). These parameters are essential for Eqs. (5)-(6) and were estimated using experimental results for HEW lysozyme from Yoda and colleagues [34], yielding $\delta_{110} = 0.63$, $\delta_{101} = 0.30$, and $K_0^+ = 0.211$. The growth rate calculation for each face utilizes kMC simulations to account for the surface microconfiguration's impact on attachment, detachment, and migration rates. The parameter γ_{edge}, defined in Eq. (2), controls the GU attachment locations, affecting the growth rates across different regimes.

Our model's predictive capability and validation are illustrated in Fig. 3. The average growth rates for the 101 and 110 faces averaged from ten independent kMC simulations under various conditions, align closely with the experimental data presented by Yoda and colleagues [34]. They showcase high fidelity, with coefficients of determination (R^2) being 0.98 for the 101 face growth and 0.96 for the 110 face growth.

To underscore our model's superiority, we compared it with the kMC model developed by Christofides and colleagues [35], which was simulated under identical conditions (black line in Fig. 3). Nayhouse's model, lacking site-specific adsorption rates, treats all lattice sites equally and adjusts parameters (K, E_{pb}, and ϕ_B) to fit experimental data at low supersaturation ($S \leq 2$). This approach, while effective for limited conditions, compromises the model's adaptability across different conditions due to its reliance on precise parameter adjustments, limiting its predictive capability without further fine-tuning for broader operating ranges. Our model excels in predicting crystal growth across three distinct regimes. These regimes are discernible in the growth rate curve, each corresponding to a specific set of conditions: rough growth, step growth, and spiral growth.

In the spiral growth regime, characterized by low supersaturation levels, the growth rate remains minimal due to the limited availability of GUs in the solution phase. Consequently, the probability of GUs adsorbing onto the crystal surface is low, resulting in sluggish growth rates. As supersaturation increases, more GUs become accessible in the solution, leading to enhanced growth rates as a greater number of GUs adsorb onto the crystal surface.

However, in the step growth regime, the growth rate curves exhibit a linear region for both (110) and (101) faces as supersaturation decreases further. This behavior aligns with observations made in other crystal growth studies, such as the growth of $n-$hexane crystals, where similar growth rate curves were divided into three regimes and a transition from smooth to rough surface growth was documented [36]. These results collectively validate the robustness and accuracy of our model in capturing the intricate dynamics of crystal growth across various regimes, reinforcing its suitability for predictive control and optimization applications in crystal growth processes.

B. Microscopic properties

The developed model serves a crucial purpose in predicting the intricate temporal variations in microscopic properties of crystal surfaces, properties that are often challenging to measure directly. In this section, we present results focusing on protein crystals of lysozymes, acknowledging that measuring properties at these scales can be exceptionally challenging. In such cases, our high-fidelity model proves invaluable in making accurate predictions.

Our simulations track the spatiotemporal evolution of the kMC lattice under specific conditions: a temperature of $277K \leq T \leq 297K$ at $5K$ intervals and a concentration of 60 mg/mL of lysozyme in water. Our observations reveal a notable trend in kink densities at various temperatures, accompanied by significant changes to the solubility of protein crystals. We also examine the temporal variations

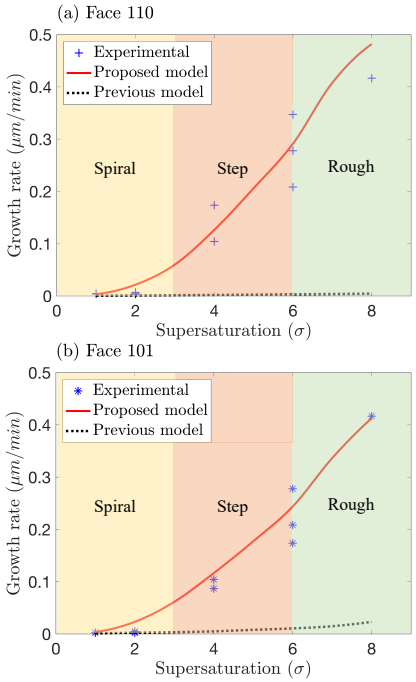

Fig. 3. Model validation for crystals at different supersaturation with different growth rates: (a) Face 110, and (b) Face 101.

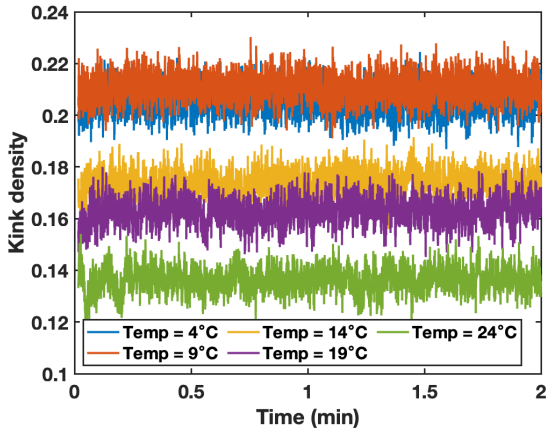

Fig. 4. Temporal evolution of kink density at different temperatures

of the kink density under varying temperature conditions. As depicted in Fig. 4, we observe the decline in the kink density becomes notably steeper at higher temperatures. Furthermore, we investigate the impact of different concentrations on the growth rates, as illustrated in Fig. 1. Evidently, increasing temperatures lead to substantial reductions in the kink density. This phenomenon is primarily attributed to the supersaturation-dependent adsorption rate of protein crystals. It also depends upon initial concentration which can further be validated using the model. These findings highlight the model's capacity to elucidate complex attachment processes and their effects on crystal properties, offering valuable insights into industrial applications such as pure larger protein crystal manufacturing.

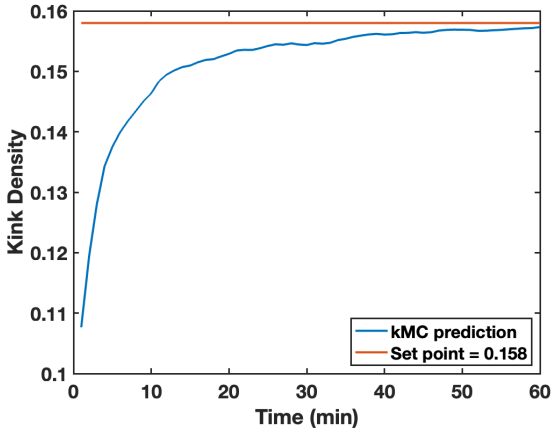

Fig. 5. Result of applying optimal input profile to kMC model.

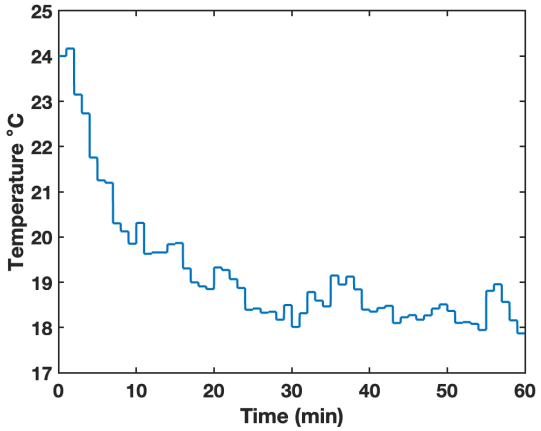

Fig. 6. The input trajectory of the temperature for the optimal operation.

C. Optimal operation

To demonstrate the remarkable setpoint tracking capability of the optimizer outlined in Eq. 9, we employed it to regulate a critical output variable: the kink density. The operational inputs encompass the reactor's temperature, concentration, and simulation time, each playing a pivotal role in determining the optimal operational strategy.

Fig. 5 vividly portrays the temporal evolution of the kink density after the application of the controller. Initially, as these figures reveal, kink density follows also a log graph due to the nature of the controller on temperature. Over time, the rate of decrease slows down, ultimately stabilizing the kink density at its setpoint.

This behavior can be readily understood by examining the temporal changes in the solution temperature input profile. Fig. 6 underscores the initial rapid decline in the temperature and increase in kink density to reach a setpoint, at the onset of the process. As time progresses, the input temperature is systematically reduced, resulting in increased attachment of kinks, subsequently increasing the attachment probabilities for kinks. These processes culminate in achieving the desired levels for the kink density in order to fine-tune growth with potential impurities during crystallization.

It is noteworthy that the input derived from the optimizer successfully guided the system output towards its setpoints,

as demonstrated in Fig. 6. The kink density achieved its setpoint, without any significant offset, albeit with minor oscillations. These oscillations arise due to the stochastic nature of the high-fidelity model introduced in Section II, which, despite minor fluctuations, highlights the optimizer's effectiveness in achieving the desired kink density value. The input profile depicted in Fig. 5 represents the optimal sequence that adheres to all constraints outlined in Eq. 9, and its application to the high-fidelity kMC model is a key element in obtaining the observed results in Fig. 6.

V. Conclusion

In our study, we developed a layered-kMC simulation model to predict crystal morphology and kink density over time, achieving high accuracy compared to experimental data for various chemical potentials. We also introduced an optimization problem to identify the best input profile including temperature, supersaturation, and crystallization time to reach a specific kink density, enhancing the purity and speed of crystal production. This optimization framework effectively maintains target values, proving its usefulness in controlling crystal growth, with implications for materials science, pharmaceuticals, and more.

References

[1] M. A. Rahim, Y. Hata, M. Björnmalm, Y. Ju, and F. Caruso, "Supramolecular metal–phenolic gels for the crystallization of active pharmaceutical ingredients," *Small*, vol. 14, no. 26, p. 1801202, 2018.

[2] N. Pudasaini, P. P. Upadhyay, C. R. Parker, S. U. Hagen, A. D. Bond, and J. Rantanen, "Downstream processability of crystal habit-modified active pharmaceutical ingredient," *Organic Process Research & Development*, vol. 21, no. 4, pp. 571–577, 2017.

[3] D. Kumar, R. Thipparaboina, and N. R. Shastri, "Impact of nisoldipine crystal morphology on its biopharmaceutical properties: A layer docking assisted study," *Organic Process Research & Development*, vol. 19, no. 12, pp. 1912–1917, 2015.

[4] N. Sitapure, T. Qiao, D. H. Son, and J. S.-I. Kwon, "Kinetic monte carlo modeling of the equilibrium-based size control of $CsPbBr_3$ perovskite quantum dots in strongly confined regime," *Computers & Chemical Engineering*, vol. 139, p. 106872, 2020.

[5] N. Sitapure, R. Epps, M. Abolhasani, and J. S.-I. Kwon, "Multiscale modeling and optimal operation of millifluidic synthesis of perovskite quantum dots: Towards size-controlled continuous manufacturing," *Chemical Engineering Journal*, vol. 413, p. 127905, 2021.

[6] N. Sitapure and J. S.-I. Kwon, "A unified approach for modeling and control of crystallization of quantum dots (QDs)," *Digital Chemical Engineering*, vol. 6, p. 100077, 2023.

[7] A. M. Kierzek and P. Zielenkiewicz, "Models of protein crystal growth," *Biophysical chemistry*, vol. 91, no. 1, pp. 1–20, 2001.

[8] N. Sitapure and J. Sang-Il Kwon, "Introducing hybrid modeling with time-series-transformers: A comparative study of series and parallel approach in batch crystallization," *Industrial & Engineering Chemistry Research*, vol. 62, no. 49, pp. 21 278–21 291, 2023.

[9] N. Sitapure and J. S.-I. Kwon, "Crystalgpt: Enhancing system-to-system transferability in crystallization prediction and control using time-series-transformers," *Computers & Chemical Engineering*, vol. 177, p. 108339, 2023.

[10] ——, "Exploring the potential of time-series transformers for process modeling and control in chemical systems: An inevitable paradigm shift?" *Chemical Engineering Research and Design*, vol. 194, pp. 461–477, 2023.

[11] P. Hartman, "Relations between structure and morphology of crystals," Ph.D. dissertation, Groningen, 1953.

[12] P. Bennema, "The importance of surface diffusion for crystal growth from solution," *Journal of Crystal Growth*, vol. 5, no. 1, pp. 29–43, 1969.

[13] Z. B. Kuvadia and M. F. Doherty, "Spiral growth model for faceted crystals of non-centrosymmetric organic molecules grown from solution," *Crystal Growth & Design*, vol. 11, no. 7, pp. 2780–2802, 2011.

[14] S. T. Yau, B. R. Thomas, and P. G. Vekilov, "Molecular mechanisms of crystallization and defect formation," *Phys. Rev. Lett.*, vol. 85, pp. 353–356, Jul 2000.

[15] P. G. Vekilov and J. I. D. Alexander, "Dynamics of layer growth in protein crystallization," *Chemical Reviews*, vol. 100, no. 6, pp. 2061–2090, 2000.

[16] K.-W. Benz, *Handbook of Industrial Crystallization*, 3rd ed. Cambridge University Press, Jun 2020, vol. 53.

[17] P. G. Vekilov, "Incorporation at Kinks: Kink Density and Activation Barriers," *AIP Conference Proceedings*, vol. 916, no. 1, pp. 235–267, 06 2007.

[18] M. Ranganathan and J. D. Weeks, "Theory of impurity induced step pinning and recovery in crystal growth from solutions," *Phys. Rev. Lett.*, vol. 110, p. 055503, Jan 2013.

[19] R. A. Vardanian and T. V. Zakarian, "Influence of impurities on kink dynamics in crystals with high peierls barriers," *Solid State Communications*, vol. 86, pp. 455–458, 1993.

[20] P. Bennema, "Spiral growth and surface roughening: Developments since burton, cabrera and frank," *Journal of Crystal Growth*, vol. 69, pp. 182–197, 1984.

[21] G. Capellades, J. O. Bonsu, and A. S. Myerson, "Impurity incorporation in solution crystallization: Diagnosis, prevention, and control," *CrystEngComm*, 2022.

[22] J. S. Kwon, M. Nayhouse, G. Orkoulas, and P. D. Christofides, "Crystal shape and size control using a plug flow crystallization configuration," *Chemical Engineering Science*, vol. 119, pp. 30–39, 2014.

[23] J. S. Kwon, M. Nayhouse, P. D. Christofides, and G. Orkoulas, "Modeling and control of crystal shape in continuous protein crystallization," *Chemical Engineering Science*, vol. 107, pp. 47–57, 2014.

[24] J. S. Kwon, M. Nayhouse, and P. D. Christofides, "Multiscale, multidomain modeling and parallel computation: Application to crystal shape evolution in crystallization," *Ind. Eng. Chem. Res.*, vol. 54, no. 47, pp. 11 903–11 914, Dec. 2015.

[25] Marcelin, M. R., "Contribution à l´étude de la cinétique physico-chimique," *Ann. Phys.*, vol. 9, no. 3, pp. 120–231, 1915.

[26] P. Ptáček, F. Šoukal, and T. Opravil, "Introduction to the transition state theory," *Introducing the Effective Mass of Activated Complex and the Discussion on the Wave Function of this Instanton*, 2018.

[27] J. J. De Yoreo and P. G. Vekilov, "Principles of Crystal Nucleation and Growth," *Reviews in Mineralogy and Geochemistry*, vol. 54, no. 1, pp. 57–93, 01 2003.

[28] D. Winn and M. F. Doherty, "A new technique for predicting the shape of solution-grown organic crystals," *AIChE Journal*, vol. 44, no. 11, pp. 2501–2514, 1998.

[29] J. W. Mullin, *Crystallization*. Elsevier, 2001.

[30] S. B. Howard, P. J. Twigg, J. K. Baird, and E. J. Meehan, "The solubility of hen egg-white lysozyme," *Journal of Crystal Growth*, vol. 90, no. 1, pp. 94–104, 1988.

[31] C. H. Lee, S. Pahari, N. Sitapure, M. A. Barteau, and J. S.-I. Kwon, "DFT–kMC analysis for identifying novel bimetallic electrocatalysts for enhanced NRR performance by suppressing HER at ambient conditions via active-site separation," *ACS Catalysis*, vol. 12, no. 24, pp. 15 609–15 617, 2022.

[32] ——, "Investigating high-performance non-precious transition metal oxide catalysts for nitrogen reduction reaction: A multifaceted DFT–kMC–LSTM approach," *ACS Catalysis*, vol. 13, no. 13, pp. 8336–8346, 2023.

[33] G. Gilmer and P. Bennema, "Simulation of crystal growth with surface diffusion," *Journal of Applied Physics*, vol. 43, no. 4, pp. 1347–1360, 1972.

[34] I. Yoshizaki, T. Sato, N. Igarashi, M. Natsuisaka, N. Tanaka, H. Komatsu, and S. Yoda, "Systematic analysis of supersaturation and lysozyme crystal quality," *Acta Crystallographica Section D*, vol. 57, no. 11, pp. 1621–1629, Nov 2001.

[35] M. Nayhouse, J. Sang-II Kwon, P. D. Christofides, and G. Orkoulas, "Crystal shape modeling and control in protein crystal growth," *Chemical Engineering Science*, vol. 87, pp. 216–223, 2013.

[36] X.-Y. Liu, P. Bennema, and J. P. van der Eerden, "Rough–flat–rough transition of crystal surfaces," *Nature*, vol. 356, no. 6372, pp. 778–780, Apr 1992.